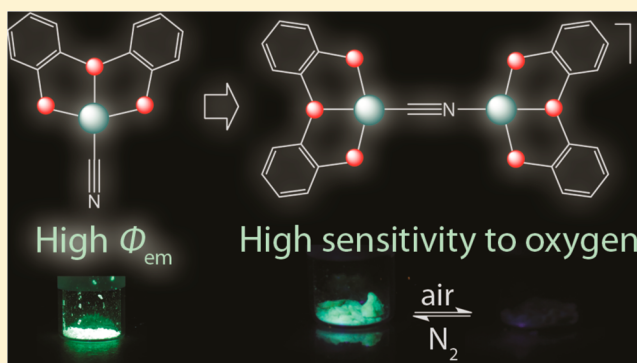


Luminescent Triphosphine Cyanide d^{10} Metal ComplexesGomathy Chakkaradhari,[†] Yi-Ting Chen,[‡] Antti J. Karttunen,[§] Minh Thuy Dau,[†] Janne Jänis,[†] Sergey P. Tunik,[#] Pi-Tai Chou,^{*,‡} Mei-Lin Ho,^{*,‡} and Igor O. Koshevoy^{*,†}[†]University of Eastern Finland, Department of Chemistry, 80101, Joensuu, Finland[‡]National Taiwan University, Department of Chemistry, Taipei 106, Taiwan[§]Aalto University, Department of Chemistry, 00076 Aalto, Finland[#]St. Petersburg State University, Department of Chemistry, Universitetskii pr. 26, 198504, St Petersburg, Russia^{*}Soochow University, Department of Chemistry, Taipei, Taiwan

Supporting Information

ABSTRACT: Coinage metal cyanides efficiently react with a triphosphine. $\text{PPh}_2\text{C}_6\text{H}_4\text{-PPh-C}_6\text{H}_4\text{PPh}_2$ (P^3), to give the complexes $\text{M}(\text{P}^3)\text{CN}$, where $\text{M} = \text{Cu}$ (1), Ag (2), and Au (3), which can further interact with coordinatively unsaturated metal centers $[\text{M}(\text{P}^3)]^+$ to give the homobimetallic $[(\text{P}^3)\text{M-CN-M}(\text{P}^3)]^+\text{X}^-$ [$\text{M} = \text{Cu}$ (4a with $\text{X}^- = \text{CF}_3\text{SO}_3^-$ and 4b with $\text{X}^- = \text{BF}_4^-$), Ag (5)] or heterometallic $[(\text{P}^3)\text{Au-CN-Ag}(\text{P}^3)]^+$ (6) species. Extension of this approach also provided the trinuclear complex $[(\text{P}^3)\text{Cu-NC-Au-CN-Cu}(\text{P}^3)]^+$ (7). Compounds 1–5 were characterized in the solid state by X-ray crystallography. The NMR spectroscopic studies revealed that all of the complexes except 6 retain their structures in solution. The title compounds are luminescent in the solid state, with quantum yields ranging from 8 to 87%. The observed photoemission originates mainly from the metal-to-ligand charge-transfer states according to time-dependent density functional theory computational studies. The crystalline bimetallic Cu complexes 4a/4b demonstrate extremely high sensitivity of the emission intensity to molecular O_2 ($K_{\text{SV1}} = 639 \text{ atm}^{-1}$ and $\text{LOD} = 0.010\%$ for 3 times the signal-to-noise ratio).



INTRODUCTION

The transition-metal complexes with d^{10} electronic configuration, which exhibit luminescence properties, have been widely exploited for the development of a variety of the photofunctional materials.¹ A large selection of ionic and neutral ligands are suitable for the preparation of light-emissive M^I compounds ($\text{M} = \text{Cu}, \text{Ag}, \text{Au}$) of different nuclearity. The latter depend on the preferable coordination number of a given metal ion (2 for Au^I and 4 for Cu^I/Ag^I). Thus, extensively studied linear Au compounds of the general formula LAuX ($\text{L} =$ phosphines, isonitriles; $\text{X} =$ halides, alkynyls, thiols, aryls) are coordinatively saturated molecules although capable of aggregation in the solid state via aurophilic bonding.² The Cu and Ag congeners of the formal LMX stoichiometry exist in the form of clusters, e.g., $\text{M}_4\text{X}_4\text{L}_4$ ($\text{L} =$ phosphine; $\text{X} =$ halides, alkynes),³ because of a pronounced tendency of these metals to adopt tetrahedral coordination geometry. The combination of a coordination vacancy and an appropriate bridging ligand (primarily iodides as X-type η^1 ligands) is a well-established way to obtain dinuclear,^{1g,k,4} trinuclear,^{1k} and other multinuclear copper halide complexes,^{4,5} some of which exhibit intriguing stimuli-responsive thermo-, vapo-, and mechano-chromic luminescence.⁶

Saturation of the coordination sites of the M^I ions ($\text{M} = \text{Cu}, \text{Ag}$) with additional donor functions diminishes the possibility of a cluster assembly and allows for the synthesis of complexes with discrete metal centers. Many of these species were reported to be efficient luminophores, employed in the fabrication of promising electroluminescent devices^{1h,7} and in the elaboration of sensing techniques.^{1c,f,8} Close attention has mainly been paid to Cu compounds, containing inexpensive and environmentally friendly metals. As a result, a series of Cu^I species with impressive photophysical characteristics were designed in the past decade.^{6e,9} Variations of the electronic properties of the ligand sphere allowed for the synthesis of compounds exhibiting very bright luminescence with tunable emission energy in the entire visible range.^{1k,9d} A decent number of experimental and theoretical works on this topic indicate that the lowest excited states of the mononuclear Cu^I complexes frequently originate from metal-to-ligand charge-transfer (MLCT) processes, accompanied by a transient oxidation, $\text{Cu}^I \rightarrow \text{Cu}^{II}$, which implies a significant change of the complex geometry.^{1a,10} A general approach to efficient Cu

Received: November 8, 2015

Scheme 1. Synthesis of Complexes 1–7

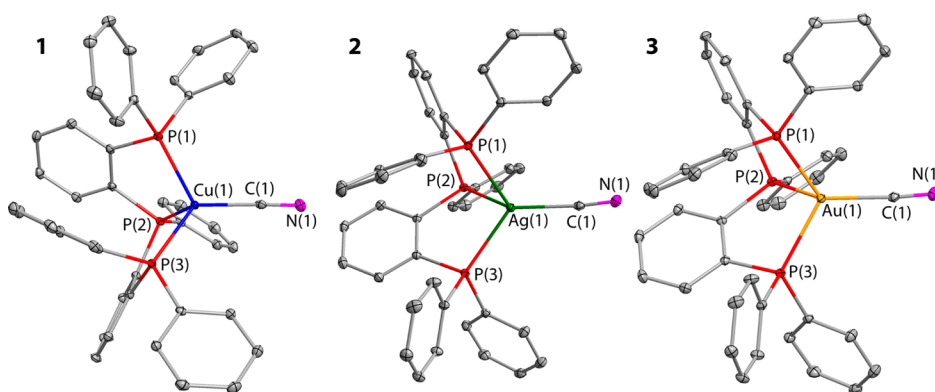
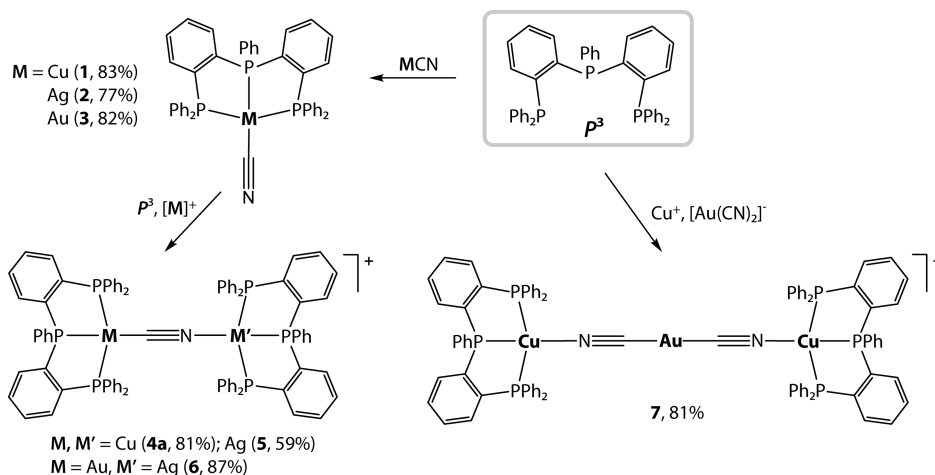


Figure 1. Molecular views of complexes 1–3. Thermal ellipsoids are shown at the 30% probability level. H atoms are omitted for clarity.

emitters involves the use of sterically crowded and rigid chelating ligands, which are thought to be important in minimizing the probability of nonradiative decay through structural relaxation from a tetrahedral to a pseudoplanar shape and therefore are beneficial in improving the quantum yield. The perspective architecture of the Cu^{I} luminophores currently resides mostly on the homo- and heterodentate diphosphine (PP) and phosphineimine (PN) ligands, combined with anionic organic (N-heterocycles)^{7d,9b,c,11} or inorganic (halides)^{1g,k,9d} groups, providing quantum yields exceeding 90% at room temperature. However, the congener Ag^{I} compounds having similar sets of ligands normally display much lower quantum efficiency,^{1a,12} with a few exceptions of moderately to highly phosphorescent silver phosphine complexes^{1h,13} and some cases of relatively strong Ag-perturbed intraligand fluorescence.¹⁴ In addition, comparative studies of isostructural complexes of d^{10} ions are scarce^{1h,12b,13c,15} presumably because of the difference in the coordination geometry of Cu^{I} , Ag^{I} , and Au^{I} .

Recently we reported utilization of a bischelating triphosphine ligand, $\text{PPh}_2\text{C}_6\text{H}_4\text{-PPh-C}_6\text{H}_4\text{PPh}_2$ [bis(*o*-diphenylphosphinophenyl)phenylphosphine, P^3], for the preparation of a family of copper(I) alkynyl compounds.¹⁶ Their emissions were mainly determined by the alkynyl ligands and had minor contributions from the metal atoms, which presumably accounted for the weak-to-moderate quantum yields in the solid state. In the current work, we describe the synthesis of highly photoemissive phosphine cyanide complexes

of group 11 metals based on the aforementioned triphosphine P^3 and further employment of the metalloligands $\text{M}(\text{P}^3)\text{CN}$ for the construction of di- and trimetallic species. The resulting compounds exhibit moderate-to-intense room temperature solid-state luminescence, the parameters of which depend strongly on the nature of the metal ion. Moreover, selected Cu complexes demonstrate highly efficient O_2 -sensing ability based on luminescence quenching in the solid state that is determined by the morphology of the crystalline samples.

RESULTS AND DISCUSSION

The mononuclear complexes $\text{M}(\text{P}^3)\text{CN}$ [$M = \text{Cu}$ (**1**), Ag (**2**), Au (**3**)] were obtained by treating the corresponding metal cyanide with a stoichiometric amount of the triphosphine to give the resulting mononuclear compounds as very pale (**1** and **2**) and yellow (**3**) solids after recrystallization in good yield (Scheme 1).

The crystal structures of 1–3 are shown in Figure 1. According to X-ray diffraction data, compounds 1–3 are isomorphous (space group $P2_1/n$), showing only slight variations of the unit cell dimensions (Table S1). The corresponding structural parameters of these complexes are also very much alike, and the noticeable alterations of the bond lengths and angles are presumably attributed to the difference in the sizes of the metal ions (Table 1), which is also reflected by the largest volume of the cell for the Ag compound **2** among these species.

Table 1. Selected Bond Lengths and Angles for Complexes 1–3

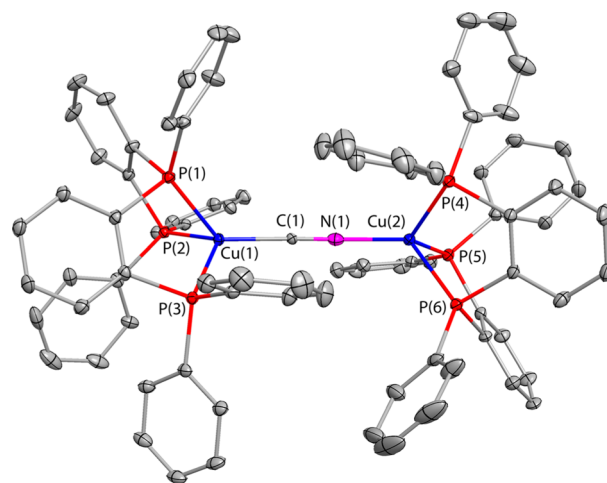
	1 (M = Cu)	2 (M = Ag)	3 (M = Au)
Bond Lengths, Å			
P(1)–M(1)	2.2948(4)	2.5277(3)	2.4016(4)
P(2)–M(1)	2.2728(5)	2.5166(4)	2.4096(5)
P(3)–M(1)	2.2891(5)	2.4841(4)	2.4138(5)
C(1)–M(1)	1.9376(17)	2.1228(13)	2.064(2)
Bond Angles, deg			
N(1)–C(1)–M(1)	178.01(15)	173.39(12)	175.57(18)
C(1)–M(1)–P(1)	120.04(5)	118.37(3)	118.80(5)
C(1)–M(1)–P(2)	123.05(5)	128.16(4)	128.84(5)
C(1)–M(1)–P(3)	117.42(5)	126.41(3)	119.30(5)
P(1)–M(1)–P(3)	114.035(16)	108.888(10)	112.913(15)
P(2)–M(1)–P(3)	87.347(16)	81.807(11)	84.197(16)
P(2)–M(1)–P(1)	87.140(16)	80.322(11)	84.442(16)

The d^{10} centers in 1–3 have a distorted tetrahedral environment in which the triphosphine ligands are bound to the metals in a tripodal mode and the remaining coordination site is occupied by a terminal cyanide group. The geometry of the complexes is therefore very similar to that found for the copper alkynyl-triphosphine complexes $\text{Cu}(\text{P}^3)\text{C}_2\text{R}$.¹⁶ The P–M bond lengths for each of the compounds do not show an appreciable deviation. For M = Cu, they are virtually the same as those in the $\text{Cu}(\text{P}^3)\text{C}_2\text{R}$ congeners but slightly longer than the corresponding values reported for other related tetracoordinate complexes.¹⁷ Ag and Au compounds structurally are very close to their chloride congeners $\text{M}(\text{P}^3)\text{Cl}$, the crystals of which were found to be nearly isomorphous to those of 2 and 3.¹⁸ The distances M–CN in 1–3 are not exceptional and fit in the range for other d^{10} cyanide complexes.^{17a,19} The Ag–CN bond is the longest metal–cyanide contact that correlates with a larger size of Ag compared to Cu and Au. IR spectra of 1–3 exhibit $\nu(\text{C}\equiv\text{N})$ stretches in the narrow range of frequencies (2108–2116 cm^{-1}), which is in line with literature data for the related compounds.^{17a}

Compounds 1–3 retain their structures in solution, which is confirmed by NMR spectroscopic studies. Complexes 1 and 3 display A_2B patterns in their ^{31}P NMR spectra, while 2 demonstrates a regular spectrum, which consists of two signals with couplings to Ag nuclei and between inequivalent P atoms; see the Experimental Section and Figure S1. Note that the signals are slightly broadened and do not show resolution of the $\text{P}^{107,109}\text{Ag}$ couplings. A characteristic low-field shift of the ^{31}P resonances in the spectra of 1–3 with respect to the free ligand indicates that all P atoms are bound to the metal centers. The ^1H NMR spectra of 1–3 are also compatible with the solid-state structures and display resolved signals of the triphosphine protons, which were assigned on the basis of 1D and ^1H – ^1H COSY experiments; see the Experimental Section and Figures S2–S4.

Potential bidentate nature of the cyanide ligands has been extensively used for the construction of a large variety of transition-metal complexes, including those built of coinage metals.^{17a,20} This bridging ability of CN^- groups prompted us to investigate the possibility of using complexes 1–3 as metalloligands in the preparation of compounds of higher nuclearity. Thus, the labile compounds $[\text{M}(\text{P}^3)]^+$, generated in situ from the phosphine and corresponding M^1 salts (M = Cu, Ag), were coupled with 1–3, which allowed for isolation of the homobimetallic $[(\text{P}^3)\text{M}–\text{CN}–\text{M}(\text{P}^3)]^+\text{X}^-$, where M = Cu (4a

with $\text{X}^- = \text{CF}_3\text{SO}_3^-$ and 4b with $\text{X}^- = \text{BF}_4^-$), Ag (5) species (Scheme 1). Attempts to prepare heterobimetallic compounds were mostly unsuccessful, resulting in the formation of homonuclear compounds both in the solid state and in solution. However, using a combination of Au and Ag ions, a mixed-metal complex, $[(\text{P}^3)\text{Au}–\text{CN}–\text{Ag}(\text{P}^3)]^+$ (6), was isolated in the crystalline state. Further extending this approach, we synthesized a trimetallic compound, $[(\text{P}^3)\text{Cu}–\text{NC}–\text{Au}–\text{CN}–\text{Cu}(\text{P}^3)]^+$ (7), in good yield by reacting a stoichiometric amount of the $[\text{Cu}(\text{P}^3)]^+$ intermediate complex with $\text{K}[\text{Au}(\text{CN})_2]$ (Scheme 1). 4a and 5 (as CF_3SO_3^- and BF_4^- salts, respectively) were characterized crystallographically in the solid state (Figures 2 and S5; selected structural parameters are listed in Table S2).

**Figure 2.** Molecular view of complex 4a. Thermal ellipsoids are shown at the 30% probability level. H atoms and counterions are omitted for clarity. One of the two independent molecules found in the unit cell is shown.

The molecular ions of bimetallic compounds 4a and 5 consist of two $\text{M}(\text{P}^3)$ fragments bridged by a cyanide group to form an approximately linear $\text{MC}\equiv\text{NM}$ chain, which is typical for CN^- bidentate coordination. The arrangement of these species resembles that of a disilver complex containing triphenylphosphine ligands $[(\text{PPh}_3)_3\text{Ag}–\text{CN}–\text{Ag}(\text{PPh}_3)_3]^+$.^{20d} The M–C and M–N distances are very close in each of complexes 4a and 5, which makes the cyanide C and N atoms virtually indistinguishable. The $\text{M}(\text{P}^3)$ moieties in 4a and 5 are structurally similar, having essentially the same geometry as their mononuclear precursors 1 and 2, respectively. Comparison of the dicopper complex 4a with its congener 1 does not reveal any substantial variations of the bond lengths and angles as a result of CN^- bridging binding. In the case of 5, however, the coupling of two Ag ions to the same cyanide ligand leads to some elongation of the Ag–C bonds (the average of Ag–C/N is 2.154 Å) compared to 1 (2.122 Å). Additionally, the Ag–P(central) bond lengths in 5 (average 2.542 Å) are increased with respect to the terminal Ag–P distances (average 2.488 Å) and to the corresponding bond in the neutral complex 2 (2.517 Å) as well.

The counterions CF_3SO_3^- and BF_4^- in the crystals of complexes 4a and 5, respectively, act as bridges connecting the nearby cationic units, which enhances the intermolecular interaction via the formation of an extended hydrogen-bonding network (Figure S6).²¹

Electrospray ionization mass spectrometry (ESI-MS) of 4–7 exhibits the dominating signals at m/z 1412.23, 1500.18, 1590.24, and 1635.20, respectively (Figure S7). The isotopic patterns fit those calculated for monocationic molecular ions, indicating that the composition of the complexes in solution is mainly retained.

Each of the dinuclear cationic species 4–6 shows a single $\nu(\text{C}\equiv\text{N})$ stretching peak in its IR spectrum between 2126 and 2137 cm^{-1} , which correspond to somewhat higher energies in comparison to their neutral relatives 1–3. The $\nu(\text{C}\equiv\text{N})$ stretching band of the trinuclear complex 7 is observed at 2172 cm^{-1} , which is indicative of the $[\text{Au}(\text{CN})_2]^-$ bridge being coordinated to the Cu ions.^{20b}

Despite the close resemblance of $\text{Cu}(\text{P}^3)$ fragments of 4a in the crystal, its ^{31}P NMR spectrum shows two distinct sets of signals, which correspond to two independent AB_2 systems (Figure 3). It apparently points to a noticeable electronic

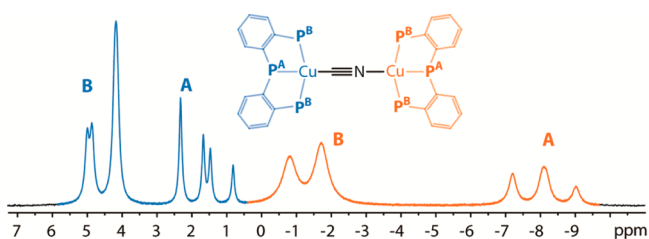


Figure 3. $^{31}\text{P}\{^1\text{H}\}$ NMR spectrum of 4a in CD_2Cl_2 at 298 K.

difference in the properties of the ligand environment in the $\text{Cu}(\text{P}^3)\text{--C}$ and $\text{Cu}(\text{P}^3)\text{--N}$ moieties of the molecule that affects shielding of the Cu and, consequently, P nuclei. The detectable inequivalence of the Cu centers also testifies to an absence of dissociation via cleavage of metal–cyanide bonds at room temperature. The low- and high-field groups of signals are tentatively assigned to C- and N-bound $\text{Cu}(\text{P}^3)$ units, respectively, on the basis of a comparison with the spectra of 1 and 7 (see also below).

In contrast to 4a, the ^{31}P NMR spectrum of the disilver complex 5 exhibits extremely small differences in the shielding of the P nuclei at C- and N-bound $\text{Ag}(\text{P}^3)$ units (see the Experimental Section and Figure S8) very probably due to the damping effect of the Ag ion electronic density and greater spatial separation of the N and C termini from the P atoms. The well-resolved splitting pattern arises from the A_2B spin system and the presence of two ^{107}Ag - and ^{109}Ag -containing isotopomers [$J(\text{P}^{\text{B}}\text{--}^{107}\text{Ag}) = 245$ Hz, $J(\text{P}^{\text{B}}\text{--}^{109}\text{Ag}) = 282$ Hz, $J(\text{P}^{\text{A}}\text{--}^{107}\text{Ag}) = 138$ Hz, and $J(\text{P}^{\text{A}}\text{--}^{109}\text{Ag}) = 195$ Hz].

The trimetallic complex 7 displays two broadened ^{31}P resonances (Figure S9) corresponding to the equivalent terminal $\text{Cu}(\text{P}^3)$ groups bound to the dicyanoaurate bridge. The chemical shifts of the signals (-0.1 and -7.0 ppm) and the coupling constant [$^3J(\text{P}\text{--}\text{P}) = 141$ Hz] are comparable with the values found for the N-bound $\text{Cu}(\text{P}^3)$ part of complex 4.

The ^1H NMR data of 4, 5, and 7 are in accordance with their structures given in Figures 2 and S5 and Scheme 1. Each of the spectra shows only one poorly resolved set of ^1H resonances that also point to an essentially weakened effect of the N and C termini on the shielding of remote aromatic rings at P-atom substituents corresponding to inequivalent P^3 ligands; see Figures S10–S12. Complexes 4a and 4b, which have different counterions, CF_3SO_3^- and BF_4^- , respectively, demonstrate

identical NMR spectroscopic characteristics, meaning that no interactions with anions occur.

The Au–Ag complex 6 did not give crystals suitable for X-ray diffraction study. According to ESI-MS and ^{31}P NMR data (Figures S7 and S13), it exists as a mixture of species in solution, although a major component can be assigned to the proposed $[(\text{P}^3)\text{Au}\text{--}\text{CN}\text{--}\text{Ag}(\text{P}^3)]^+$ composition. Numerous recrystallizations of the sample did not affect the appearance of the ^{31}P NMR spectrum, which points to dynamic equilibrium of the species presented in the fluid medium. The sharp low-field resonances can be assigned to the AB_2 spin system of the $(\text{P}^3)\text{Au}$ group, which resembles the corresponding spectrum of 3. The signals in the high-field part of the spectrum belong to the Ag-coordinated triphosphine. However, the number of signals and their multiplicity cannot be explained in terms of a single type of $\text{Ag}(\text{P}^3)$ -containing species, indicating possible formation of, e.g., 2 and/or 5, due to dissociation of the silver–cyanide and gold–cyanide bonds. This hypothesis is also supported by the presence of intense peaks in ESI-MS of 6, which can be assigned to the cation 5. Upon crystallization of 6, a uniform solid, presumably consisting of the only type of molecular ion $[(\text{P}^3)\text{Au}\text{--}\text{CN}\text{--}\text{Ag}(\text{P}^3)]^+$, is quantitatively formed. The selectivity of this process and phase purity are confirmed by the physical properties of this material, which are very different from those of the potential admixtures 2 and 5 (see the section below).

Photophysical Properties and Computational Studies.

The photophysical data of the complexes under study are summarized in Table 2. Absorption spectra of 1–7 in CH_2Cl_2 are shown in Figure S14. Each of the complexes displays a major broad band with a maximum found in the range 260–350 nm, which may be assigned to the triphosphine $\pi\text{--}\pi^*$ intraligand transition by analogy with other tetrahedral

Table 2. Photophysical Properties of Complexes 1–7 at 298 K

	solid ^a				solution ^b		
	$\lambda_{\text{em}}, \text{nm}$	$\tau_{\text{obs}}, \mu\text{s}$	$k_{\text{tr}}, \text{s}^{-1}$	Φ	$\lambda_{\text{abs}}, \text{nm}$ ($\epsilon \times 10^4, \text{M}^{-1} \text{cm}^{-1}$)	$\lambda_{\text{em}}, \text{nm}$	$\Phi \times 10^3$
1	530	15.41	4.5×10^4	0.70	300 (2.5)	665	0.7
2	525	29.23	3.0×10^4	0.87	285 (2.7)	675	0.8
3	640	1.38	5.8×10^4	0.08	315 (3.0)		
4a	520	1.31 ns (24.42%), 44.84 ns (75.58%)		0	295 (3.7)	640	2.0
4b	520	58.4 ns (50.65%), 2.44 μs (49.35%)		0	295 (3.8)	640	2.1
5	510	5.59	2.7×10^4	0.15	285 (6.6)	650	1.9
6	590	3.44	8.1×10^4	0.28	285 (6.1)	650	1.0
7	545	5.64	3.7×10^4	0.21	295 (9.4)	640	2.3

^aIn air, $\lambda_{\text{exc}} = 406$ nm; the uncertainty of the quantum yield measurement was in the range of $\pm 5\%$ (an average of three replications). ^bIn a degassed CH_2Cl_2 solution, $\lambda_{\text{exc}} = 355$ nm. ^c k_{tr} was estimated by Φ/τ_{obs} .

compounds.^{17b} The bands extend to ca. 350–480 nm, presumably because of the presence of weak unresolved shoulders resulting from the electronic transitions ($\epsilon < 5 \times 10^4 \text{ M}^{-1} \text{ cm}^{-1}$), which may have contributions from the spin-allowed ¹MLCT, which involves the constituting metal ions and cyanide and phosphine ligands.

Compounds 1–7 exhibit a very weak luminescence in a degassed solution at 298 K (Figure S15 and Table 2), showing low quantum yields from 7×10^{-4} to 2×10^{-3} , while complex 3 is virtually nonemissive. In comparison with the solid-state data, the emission bands of complexes 1–7 in CH_2Cl_2 are significantly red-shifted by ca. 110 nm. This simultaneous decrease of the emission energy and quantum efficiency was earlier explained by flattening distortions of the d^{10} complex pseudotetrahedral geometry that occur after MLCT excitation and result in the appearance of effective nonradiative relaxation pathways of the excited state in a nonrigid environment.^{9b,13a,b,17b,22}

Figure 4 shows the solid-state emission spectra of 1–3 and 5–7 at 298 K, as well as the excitation spectra acquired by

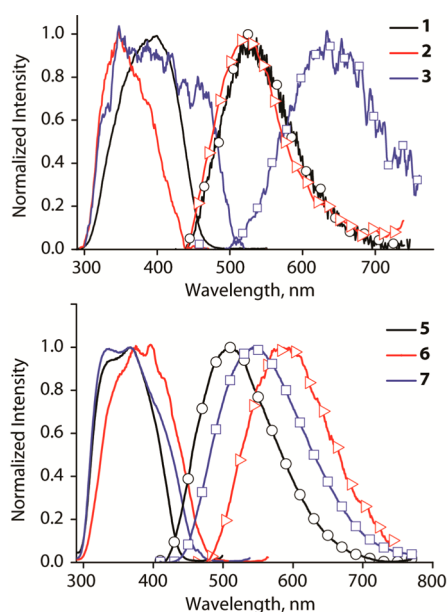


Figure 4. Normalized solid-state excitation (solid line) and emission (solid line plus symbol) spectra of 1–3 and 5–7 at 298 K. $\lambda_{\text{ex}} = 406$ nm for emission. The excitation spectra were acquired by monitoring the emission at the peak wavelength. Also, it should be noted that the excitation spectra have been distorted at short wavelength (e.g., <400 nm) because of the prepared thick solid sample.

monitoring the emission at the peak wavelength. The mononuclear compounds 1 and 2 display very strong green emission with quantum yields of 0.70 and 0.87, respectively. It is worth mentioning that the luminescence intensity of the copper cyanide complex 1 is more than 3 times larger than the maximum quantum yield Φ that we observed for the congener alkynyl $\text{Cu}(\text{P}^3)\text{C}_2\text{R}$ species.¹⁶

To the best of our knowledge, the room temperature efficiency of 2 in the solid state is the highest one among the monometallic Ag^{I} luminophores to date. The relatively long lifetimes of 1 and 2 (15.41 and 29.23 μs) are considerably longer than the τ values typical for Cu^{I} and Ag^{I} complexes exhibiting thermally activated delayed fluorescence.^{14,h,9b,23} In contrast to 1 and 2, the Au complex 3 shows a broad and much

red-shifted emission band (640 nm) with a low quantum yield ($\Phi = 0.08$). Similar behavior was recently described among the series of $\text{M}(\text{PP})(\text{PS})$ ($\text{M} = \text{Cu}, \text{Ag}, \text{Au}$) complexes [PP = 1,2-bis(diphenylphosphino)benzene; PS = 2-diphenylphosphino-benzenethiolate].^{1h} The weak emission, in our viewpoint, in part, can be ascribed to the energy gap law,²⁴ which specifies that the rate constant for radiationless deactivation, k_{nr} , between two states (generally excited and ground states) in the absence of a zero-order surface crossing can be assessed by $k_{\text{nr}} \sim \nu e^{-\alpha \Delta E}$, where α is a proportionality constant and ΔE denotes the emission energy gap. Accordingly, the rather small ΔE induces drastic radiationless deactivation, resulting in weak emission intensity.

The emission bands of the dinuclear complexes 4a, 4b, and 5 are slightly blue-shifted compared to those of the mononuclear compounds 1 and 2.

The heterobimetallic compound 6, which demonstrates dynamic behavior in solution resulting in the formation of several species, however, upon crystallization gives a uniform crystalline material. The emission maximum is located at 590 nm, which is somewhere between the values of the Ag and Au congeners 2 and 3 (525 and 640 nm, respectively). The disilver complex 5, detected as a second major component in a solution of 6 (see Figures S7 and S13 for the MS and ³¹P NMR spectra), is virtually absent in the solid sample of 6. This is proven by the shape of the emission profile of 6 because no shoulder around 510 nm arising from 5 can be identified. The uniformity of the phase of 6 is also confirmed by the decay time, which gives a lifetime different from that of 5. The luminescence properties of the trinuclear complex 7 are dominated by the $\{\text{Cu}(\text{P}^3)\}^+$ units. The emission band ($\lambda_{\text{em}} = 545$ nm) is similar to the wavelength of the dicopper relatives 4a and 4b (see Table 2).

To elucidate the photophysical properties of the d^{10} metal complexes 1–7, we investigated their structural and electronic characteristics with quantum-chemical methods. The geometries of the studied complexes were fully optimized at the DFT-PBE0 level of theory, and the excited states were studied by means of time-dependent density functional theory calculations (TDDFT-PBE0; see the Experimental Section for full computational details). The optimized geometries of complexes 1–5 are in good agreement with the available X-ray structures (the coordinates of the optimized structures are included in the Supporting Information).

The wavelengths predicted for the $\text{S}_0 \rightarrow \text{S}_1$ and $\text{T}_1 \rightarrow \text{S}_0$ electronic transitions of all studied complexes are listed in Table 3, and the $\text{T}_1 \rightarrow \text{S}_0$ electron density difference plots are shown in Figure 5 for complexes 1, 4, and 7 (the $\text{S}_0 \rightarrow \text{S}_1$ plots are not included because they are practically analogous to the $\text{T}_1 \rightarrow \text{S}_0$ plots shown here).

The electron density difference plots of the complexes 2, 3, 5, and 6 are illustrated in Figure S16. The predicted $\text{S}_0 \rightarrow \text{S}_1$ excitation energies are generally in line with the experimental results. The larger excitation wavelengths of complexes 3 and 6 are reproduced qualitatively, while the excitation wavelength of complex 7 is clearly underestimated. The $\text{T}_1 \rightarrow \text{S}_0$ emission wavelengths listed in the table are also in qualitative agreement with the experiment, with complexes 3 and 6 again showing the largest wavelengths. For all studied complexes, the lowest-energy excited state can be described as MLCT delocalized over the triphosphane ligand. The CN ligand also contributes for 1–6. This assignment differs from that suggested for the alkynyl congeners of the titled compounds,¹⁶ for which the intraligand and ligand-to-ligand (LLCT) charge transfers

Table 3. Computational Photophysical Results for the d^{10} Metal Complexes 1–7 in the Gas Phase (TDDFT-PBE0)^a

	$\lambda(S_0 \rightarrow S_1)$, nm		$\lambda(T_1 \rightarrow S_0)$, nm	
	theor.	exp. ^b	theor.	exp. ^b
1	401	415	533	530
2	406	400	544	525
3	471	459	702	640
4	371	405	446	520
5	372	405	463	510
6	416	450	575	590
7	341	415	479	545

^a $\lambda(S_0 \rightarrow S_1)$ values are TDDFT vertical excitations. $\lambda(T_1 \rightarrow S_0)$ values are plain HOMO–LUMO gaps at the optimized T_1 geometry for 1–6 and TDDFT vertical (de)excitation for 7 (see the [Computational Details](#) section). ^bExcitation and emission wavelengths from the solid state at 298 K.

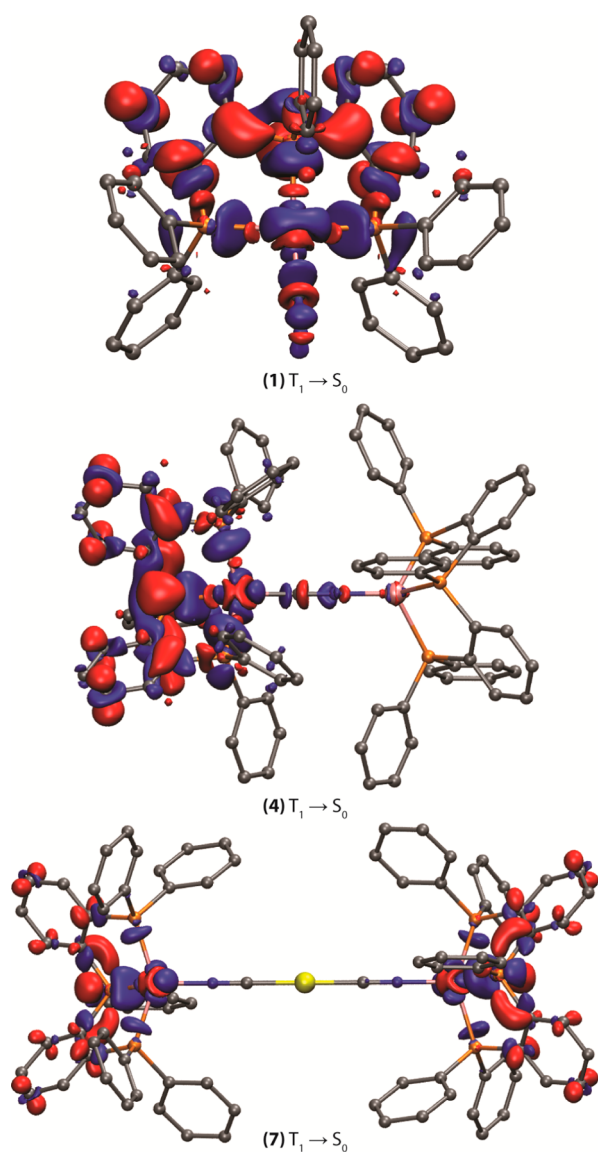


Figure 5. Electron density difference plots for the lowest-energy triplet emission ($T_1 \rightarrow S_0$) of complexes 1, 4, and 7 (isovalue 0.002 au). During the electronic transition, the electron density increases in the blue areas and decreases in the red areas. H atoms are omitted for clarity.

dominated according to the theoretical studies. The difference in the electronic structures is also reflected by the blue shift and much higher quantum yield of emission of 1 and 4 compared to their alkynyl relatives.

Molecular O_2 Sensing by Complexes 4a and 4b. The Cu^I compounds proved to be suitable for photoluminescent O_2 sensing both on support materials²⁵ and in a pure form.^{8b,25b,26} The mechanism of the process is based on quenching of the complex triplet excited state by the ground-state triplet O_2 as a result of bimolecular collisions that leads to a nonradiative relaxation of a phosphor. Previous studies on luminescent materials for O_2 sensing have principally focused on rare metal-based phosphors (iridium, platinum, etc.)²⁷ because of efficient spin–orbit coupling. The d^{10} coinage metal complexes such as Cu^I complexes are more attractive than other metal complexes as luminescent sensors because of their unique electronic structure, long emission decay time, low cost, low toxicity, and abundance. Accordingly, the crystals of complexes 4a and 4b show significant O_2 -dependent emission properties. 4a and 4b are brightly emissive under an inert atmosphere or in vacuum [$\lambda_{em} = 520$ nm; $\tau_{obs} = 6.27$ μs (4a) and 8.62 μs (4b)], whereas under aerated conditions, the complexes show very weak luminescence with significantly shortened lifetimes (44.84 and 1.31 ns for 4a and 2.44 μs and 58.4 ns for 4b). The corresponding results are summarized in [Figure 6](#) and [Tables 2](#) and 4, and details are described as follows.

At 1 atm of O_2 , the emission intensity of 4a is very largely quenched by 99.05% ([Figure 6a](#)). This response is somewhat higher than that of the effective $[Cu(\text{isocyanide})_2(\text{phen})]^+$ systems^{8b} but lower than the value recently reported for the copper azolate framework.^{26b} The Stern–Volmer (SV) plot of the signal intensity versus O_2 concentration is not linear because of the possible heterogeneity of the material and can be fitted by a two-site model^{25b} expressed by the following equation ([Figure 6c](#)):

$$\frac{I_0}{I} = \left(\frac{f_1}{1 + K_{SV1}[O_2]} + \frac{f_2}{1 + K_{SV2}[O_2]} \right)^{-1}$$

where f_1 and f_2 ($f_1 + f_2 = 1$) are the fractions of emission generated by each of the components, which experience different quenching, and K_{SV1} and K_{SV2} are the SV constants for these components. The fitting parameters given in [Table 4](#) indicate a very small fraction of component 2 ($f_2 = 0.008$, i.e., 0.8%), which is poorly quenched by O_2 ($K_{SV2} = 0.2$ atm⁻¹). Compound 4a shows excellent sensitivity to O_2 ($K_{SV1} = 319$ atm⁻¹), which is 3 times higher than the best result achieved by mononuclear Cu^I compounds reported so far ($K_{SV} = 96$ atm⁻¹)^{8b} and is comparable to the extreme properties of the copper azolate polymer ($K_{SV} = 356$ atm⁻¹).^{26b} The photoluminescence measurements were carried out upon repetitive changes of the atmosphere from pure O_2 to N_2 by purging the microcrystalline sample 4a with the corresponding gas. The intensity response ([Figure 6e](#)) testifies to the fast and reversible response of the system that quickly reaches equilibrium, as well as its decent photochemical stability. One of the reasons why phosphorescent metal complexes demonstrate O_2 sensing ability is the presence of a sufficient void space within the bulk solid that allows O_2 to penetrate into the material and to quench the luminescence provided the excited-state lifetimes are long enough for collisional interactions to occur.^{26b} Analysis of the X-ray structure of 4a shows that the potential solvent area constitutes 13.2% of the unit cell [Brunauer–Emmett–

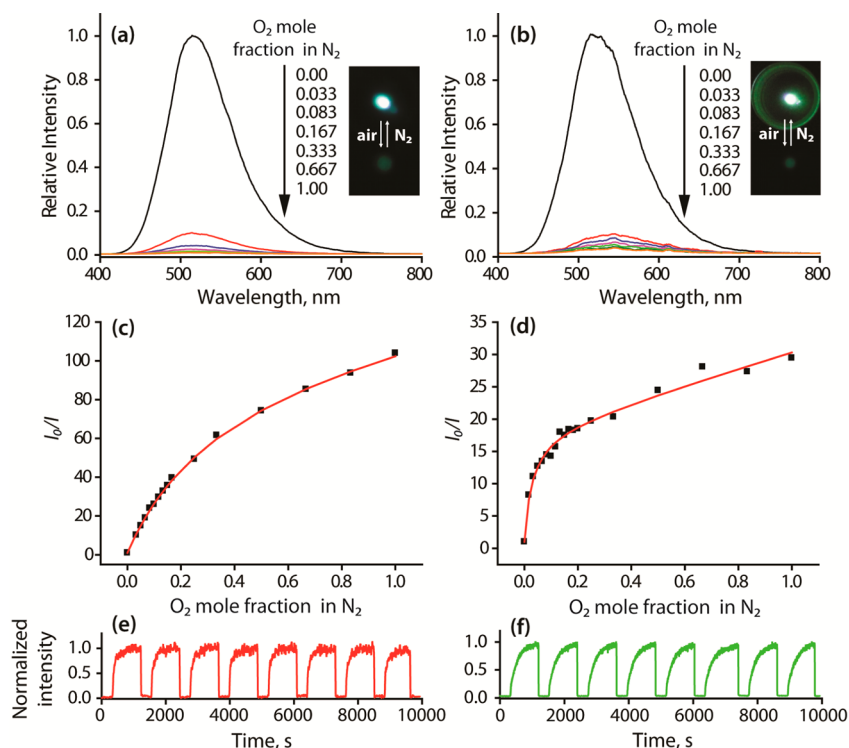


Figure 6. Emission spectra of complexes **4a** (a) and **4b** (b) under different concentrations of O_2 . (c and d) Corresponding SV plots of **4a** and **4b**. (e and f) Intensity response during variation between 1 atm of N_2 and 1 atm of O_2 .

Table 4. O_2 -Quenching Fitting Parameters of the Crystalline **4a** and **4b** Complexes^a

compound	K_{SV} (f) ^b	R^2	95% response time, s	95% recovery time, s	LOD, %
4a	319 (0.992), 0.2 (0.008)	0.9987	25	256	0.012
4b	639 (0.948), 0.66 (0.052)	0.9968	24	388	0.010

^aThe emission was detected at 298 K upon excitation at 405 nm.

^bThe data in parentheses indicate the fractions of emission generated by each of the components.

Teller (BET) and Langmuir surface areas: 258 and 344 $m^2 g^{-1}$], which is significantly larger than the void space values (2–4%) found for other Cu complexes.^{8b,26a}

Changing the counterion to BF_4^- (**4b**) provided a material with more developed porosity (BET and Langmuir surface areas: 352 and 462 $m^2 g^{-1}$). Analogous to **4a**, the SV plot for **4b** was treated using a two-site approach (Figure 6d). The sensitivity has double the reaching constant K_{SV1} of 639 atm^{-1} , which is an unprecedented value for unsupported materials (Figure 6d). The minimum detectable concentrations (LODs) of O_2 for **4a** and **4b** were calculated to be 0.012% and 0.010%, respectively, from 3 times the signal-to-noise ratio. Alternatively, it corresponds to the values of 0.037 and 0.023 mbar, respectively, at 1% quenching. This sensitivity is visibly higher than that recently reported for porous the copper(I) triazolite framework (0.047 mbar), termed the “extraordinary oxygen-sensing performance”.^{26b}

CONCLUSIONS

A series of triphosphine P^3 -supported cyanide complexes of d^{10} coinage metals were prepared. Using the potential bidentate

nature of the CN^- group, the mononuclear compounds $M(P^3)CN$ [$M = Cu$ (**1**), Ag (**2**), Au (**3**)] served as metalloligands and afforded the dinuclear ($[(P^3)M-CN-M(P^3)]^+$, **4–6**) and trinuclear ($[(P^3)Cu-NC-Au-CN-Cu(P^3)]^+$, **7**) species. Complexes **1–5** were characterized crystallographically and revealed essentially similar pseudotetrahedral coordination geometry of the metal centers bearing P^3 ligands. All of the title compounds are virtually nonemissive in solution but demonstrate moderate-to-intense room temperature photoluminescence in the solid state, $\Phi_{em} = 8\%$ (**3**) to 87% (**2**), with the latter being the highest value for mononuclear Ag^I luminophores reported to date. TDDFT computational analysis of the electronic structures of **1–6** indicates that the observed luminescence is mainly governed by MLCT processes delocalized over the triphosphane ligand and mixed with some LLCT.

The dinuclear Cu complexes **4a/4b** form the crystalline materials with a large content of crystallization solvent, the removal of which provides the solids with considerable surface areas. The availability of the suitable pores and the developed void space within the bulk solid of **4a/4b** result in a very high sensitivity of luminescence to molecular O_2 (K_{SV1} of 639 atm^{-1} and LOD = 0.010% for 3 times the signal-to-noise ratio for **4b**), which efficiently quenches the phosphorescence of **4a/4b** via triplet–triplet annihilation provided by collisional interactions.

EXPERIMENTAL SECTION

General Comments. (2-Bromophenyl)diphenylphosphine was prepared according to the reported procedure.²⁸ Other reagents were used as received. The solution 1H , $^{31}P\{^1H\}$, and $^1H-^1H$ COSY NMR spectra were recorded on Bruker 400 MHz Avance and AMX 400 spectrometers. MS spectra were measured on a Bruker APEX-Qe Qh-FT-ICR mass spectrometer in the ESI^+ mode. Microanalyses were carried out at the analytical laboratory of the University of Eastern Finland.

Bis(2-diphenylphosphinophenyl)phenylphosphine (P^3). The ligand was obtained according to a modified procedure²⁹ to give a considerably higher yield. The synthesis was carried out under a nitrogen atmosphere. A solution of (2-bromophenyl)-diphenylphosphine (1.2 g, 3.53 mmol) in tetrahydrofuran (20 cm³) was cooled to -78 °C, and a 1.6 M solution of *n*-BuLi (2.2 cm³, 3.52 mmol) was added dropwise within 10 min. The resulting orange solution was stirred for 1 h at this temperature and treated dropwise with PPhCl₂ (0.315 g, 1.76 mmol). The reaction mixture was stirred below -70 °C for 1 h, then allowed (ca. 2 h) to slowly reach room temperature, and additionally stirred for 3 h. The reaction was quenched with methanol (5 cm³), the solvents were evaporated, and the yellow amorphous residue was washed with methanol (5 × 15 cm³) to give a white solid of sufficient purity (0.95 g, 86%). ³¹P{¹H} NMR (CDCl₃; 298 K; δ): AB₂ system -15.2 (2P), -18.9 (1P) [$J(P-P) = 153$ Hz]. ¹H NMR (CDCl₃; 298 K; δ): 7.26–7.10 (m, 31H), 6.86 (m, 2H).

Caution! Metal cyanides are very toxic and dangerous for the environment.

Cu(P^3)CN (1). P^3 (100 mg, 0.159 mmol) and CuCN (14 mg, 0.159 mmol) were suspended in dichloromethane (10 cm³), and the reaction mixture was stirred for 10 h at room temperature to give a nearly clear pale-yellow solution. It was filtered and evaporated, and the crude solid was recrystallized by gas-phase diffusion of diethyl ether into a dichloromethane solution of **1** at 5 °C to give a pale-green crystalline material (95 mg, 83%). ³¹P{¹H} NMR (CD₂Cl₂; 298 K; δ): AB₂ system 2.7 (2P), -0.2 (1P) [$J(P-P) = 127$ Hz]. ¹H NMR (CD₂Cl₂; 298 K; δ): PPh₂ groups 7.89 (m, 4H, *o*-H), 7.4 (dm, 4H, *m*-H), 7.39 (m, 2H, *p*-H), 7.26 (t, 2H, $J(H-H) = 7.4$ Hz, *p*-H), 7.06 (dd, 4H, $J(H-H) = 7.7$ and 7.4 Hz, *m*-H), 6.61 (dm, 4H, $J(H-H) = 7.7$ Hz, *o*-H); C₆H₄ groups 7.72 (dm, 2H, $J(H-H) = 7.0$ Hz, *o*-H), 7.51 (dd, 2H, $J(H-H) = 7.4$ and 7.0 Hz, *m*-H), 7.39 (dd, 2H, $J(H-H) =$ ca. 7.0 Hz, *m*-H), 7.31 (dm, 2H, $J(H-H) =$ ca. 7.0 Hz, *o*-H, C₆H₅); PPh group 7.22–7.38 (m, 5H). IR [KBr; $\nu(CN)$; cm⁻¹]: 2108. Anal. Calcd for C₄₃H₃₃CuNP₃: C, 71.71; H, 4.61; N, 1.94. Found: C, 71.55; H, 4.53; N, 1.98.

Ag(P^3)CN (2). The complex was prepared analogously to **1** using AgCN (21 mg, 0.159 mmol) and P^3 (100 mg, 0.159 mmol). Recrystallization by slow evaporation of a dichloromethane/acetonitrile solution at 5 °C gave colorless crystals of **2** (92 mg, 77%). ³¹P{¹H} NMR (CD₂Cl₂; 298 K; δ): -5.7 (dd br, 2P, $J(P-P) = 193$ Hz, $J_{av}(P-Ag) =$ ca. 205 Hz), -21.0 dt (1P, $J(P-P) = 193$ Hz, $J_{av}(P-Ag) = 144$ Hz). ¹H NMR (CD₂Cl₂; 298 K; δ): PPh₂ groups 7.59 (m, 4H, *o*-H), 7.34 (m, 4H, *m*-H), 7.32 (m, 2H, *p*-H), 7.29 (m, 2H, *p*-H), 7.18 (m, 4H, *m*-H), 6.89 (m, 4H, *o*-H); other groups 7.05–7.40 (m, 13H). IR (KBr; $\nu(CN)$; cm⁻¹): 2116. Anal. Calcd for C₄₃H₃₃AgNP₃: C, 67.55; H, 4.35; N, 1.83. Found: C, 67.16; H, 4.36; N, 1.87.

Au(P^3)CN (3). The complex was prepared analogously to **1** using AuCN (63 mg, 0.280 mmol) and P^3 (185 mg, 0.294 mmol). Recrystallization by the slow evaporation of a dichloromethane/toluene solution at 5 °C gave bright-yellow crystals of **3** (198 mg, 82%). ³¹P{¹H} NMR (CD₂Cl₂; 298 K; δ): AB₂ system 14.2 (2P), 8.9 (1P) [$J(P-P) = 169$ Hz]. ¹H NMR (CD₂Cl₂; 298 K; δ): PPh₂ groups 7.82 (m, 4H, *o*-H), 7.45 (m, 6H, *m*+*p*-H), 7.27 (t, 2H, $J(H-H) = 8.0$ Hz, *p*-H), 7.06 (dd, 4H, $J(H-H) = 8.0$ and 7.6 Hz, *m*-H), 6.66 (dm, 4H, *o*-H, $J(H-H) = 8.0$ Hz); C₆H₄ 7.83 (m, 2H, *m*-H), 7.48 (m, 2H, *o*-H), 7.39 (m, 4H, *m*+*o*-H); PPh 7.35 (t, 1H, $J(H-H) = 7.5$ Hz, *p*-H), 7.28 (dd, 2H, $J(H-H) = 7.9$ and 7.5 Hz, *m*-H), 7.19 (dd, 2H, $J(H-H) = 7.9$ Hz, $J(H-P) = 11.0$ Hz, *o*-H). IR (KBr; $\nu(CN)$; cm⁻¹): 2112. Anal. Calcd for C₄₃H₃₃AuNP₃: C, 60.50; H, 3.89; N, 1.64. Found: C, 60.19; H, 3.98; N, 1.66.

[Cu(P^3)CNCu(P^3)](CF₃SO₃) (4a**).** P^3 (50 mg, 0.079 mmol) and CuCN (7 mg, 0.078 mmol) were suspended in dichloromethane (10 cm³), and the reaction mixture was stirred for 1 h at room temperature. Then a solution of P^3 (50 mg, 0.079 mmol) and [Cu(NCMe)₄](CF₃SO₃) (29 mg, 0.077 mmol) in dichloromethane (10 cm³) was added. The reaction mixture was stirred for an additional 10 h to give a clear pale-yellow solution. It was filtered and evaporated, and the crude solid was recrystallized by the slow evaporation of a dilute CH₂Cl₂/ethyl acetate/heptane solution of **4a** at room

temperature to give pale-yellow block crystals (98 mg, 81%). ESI-MS (m/z): [M]⁺ 1412.23 (calcd 1412.22). ³¹P{¹H} NMR (CD₂Cl₂; 298 K; δ): AB₂ system 1 4.4 (2P), 1.7 (1P), [$J(P-P) = 126$ Hz]; AB₂ system 2 -1.4 (br, 2P), -8.1 (br, 1P) [$J(P-P) = 146$ Hz]. ¹H NMR (CD₂Cl₂; 298 K; δ): PPh₂ groups 7.72 (m, 8H, $J(H-H) = 8.0$ Hz, *o*-H), 7.32 (t, 4H, $J(H-H) = 7.9$ Hz, *p*-H), 7.11 (m, 8H, $J(H-H) = 7.6$ and 7.9 Hz, *m*-H), 7.09 (t, 4H, $J(H-H) = 7.6$ Hz, *p*-H), 6.84 (dd, 8H, $J(H-H) = 7.6$ and 8.0 Hz, *m*-H), 6.58 (m, 8H, $J(H-H) = 7.6$ Hz, *o*-H); C₆H₄ groups 7.74 (m, 4H, $J(H-H) = 7.5$ Hz, *o*-H), 7.57 (dd, 4H, $J(H-H) = 7.5$ and 7.8 Hz, *m*-H), 7.48 (dd, 4H, $J(H-H) = 7.6$ and 7.8 Hz, *m*-H), 7.32 (m, 4H, $J(H-H) = 7.6$ Hz, *o*-H); PPh groups 7.28 (t, 2H, $J(H-H) = 7.6$ Hz, *p*-H), 7.06–7.17 (m, 8H, *o*+*m*-H). IR (KBr; $\nu(CN)$; cm⁻¹): 2133. Anal. Calcd for C₈₆H₆₆Cu₂F₃NO₃P₆S: C, 66.07; H, 4.26; N, 0.90. Found: C, 65.73; H, 4.28; N, 0.82.

The complex with the BF₄⁻ counterion (**4b**) was prepared analogously to **4a** using [Cu(NCMe)₄](BF₄); recrystallization via gas-phase diffusion of diethyl ether into CH₂Cl₂/methanol solution at 298 K gave pale-yellow block crystals (78%). NMR data of **4b** are identical with those of **4a**. IR (KBr; $\nu(CN)$; cm⁻¹): 2133. Anal. Calcd for C₈₅H₆₆BCu₂F₄NP₆: C, 68.01; H, 4.43; N, 0.93. Found: C, 67.82; H, 4.51; N, 0.87.

[Ag(P^3)CNAg(P^3)](BF₄) (5**).** P^3 (50 mg, 0.079 mmol) and AgCN (10.5 mg, 0.078 mmol) were suspended in dichloromethane (10 cm³), and the reaction mixture was stirred for 1 h at room temperature. Then P^3 (50 mg, 0.079 mmol) was added, followed by a solution of AgBF₄ (15 mg, 0.077 mmol) in acetone (5 cm³). The reaction mixture was stirred for an additional 10 h to give a clear pale-yellow solution. It was filtered and evaporated, and the crude solid was recrystallized by gas-phase diffusion of diethyl ether into a CH₂Cl₂ solution of **5** at 278 K to give colorless block crystals (72 mg, 59%). ESI-MS (m/z): [M]⁺ 1500.18 (calcd 1500.17). ³¹P{¹H} NMR (CD₂Cl₂; 298 K; δ): AB₂ spin system -5.0 (2P, $^3J(P-P) = 195$ Hz, $J(P-^{107}Ag) = 245$ Hz, $J(P-^{109}Ag) = 282$ Hz), -22.0 (1P, $^3J(P-P) = 195$ Hz, $J(P-^{107}Ag) = 138$ Hz, $J(P-^{109}Ag) = 160$ Hz). ¹H NMR (CD₂Cl₂; 298 K; δ): PPh₂ groups 7.56 (dd, 8H, $J(H-H) = 7.2$ Hz, $J(H-P) = 11.0$ Hz, *o*-H), 7.33 (t, 4H, $J(H-H) = 7.8$ Hz, *p*-H), 7.20 (dd, 8H, $J(H-H) = 6.8$ and 7.8 Hz, *m*-H), 7.19 (t, 4H, $J(H-H) = 7.8$ Hz, *p*-H), 7.07 (dd, 8H, $J(H-H) = 7.2$ and 7.8 Hz, *m*-H), 6.89 (dd, 8H, $J(H-H) = 6.8$ Hz, $J(H-P) = 11.5$ Hz, *o*-H); C₆H₄ 7.43 (m, 4H, *m*-H), 7.41 (m, 4H, *o*-H), 7.33 (dm, 4H, $J(H-H) = 7.0$ Hz, *m*-H), 7.11 (m, 4H, $J(H-H) = 7.0$ Hz, *o*-H); PPh 7.30 (m, 2H, *p*-H), 7.18 (m, 4H, *m*-H), 7.10 (m, 4H, *o*-H). IR (KBr; $\nu(CN)$; cm⁻¹): 2137. Anal. Calcd for C₈₅H₆₆Ag₂BF₄NP₆: C, 64.21; H, 4.18; N, 0.88. Found: C, 63.89; H, 4.55; N, 1.05.

[Ag(P^3)CNAu(P^3)](CF₃SO₃) (6**).** P^3 (50 mg, 0.079 mmol) and AuCN (17 mg, 0.076 mmol) were suspended in dichloromethane (10 cm³), and the reaction mixture was stirred for 1 h at room temperature. Then P^3 (50 mg, 0.079 mmol) was added, followed by a solution of AgCF₃SO₃ (20 mg, 0.078 mmol) in acetone (5 cm³). The reaction mixture was stirred for an additional 10 h to give a clear pale-yellow solution. It was filtered and evaporated, and the crude solid was recrystallized by gas-phase diffusion of diethyl ether into a CHCl₃ solution of **6** at 298 K to give a yellow crystalline material (115 mg, 87%). ESI-MS (m/z): [M]⁺ 1590.24 (calcd 1590.23). NMR spectra show the presence of several species; see the discussion. IR (KBr; $\nu(CN)$; cm⁻¹): 2126. Anal. Calcd for C₈₆H₆₆AgAuF₃NO₃P₆S: C, 59.32; H, 3.82; N, 0.80. Found: C, 58.98; H, 3.71; N, 0.57.

[Cu(P^3)NC₂Au](CF₃SO₃) (7**).** P^3 (80 mg, 0.127 mmol) and [Cu(NCMe)₄](CF₃SO₃) (48 mg, 0.127 mmol) were suspended in dichloromethane (10 cm³), and the reaction mixture was stirred for 1 h at room temperature. Then a solution of K[Au(CN)₂] (18 mg, 0.063 mmol) in methanol (5 cm³) was added. The reaction mixture was stirred for an additional 10 h to give a clear pale-yellow solution. It was filtered and evaporated, and the crude solid was recrystallized by the slow evaporation of a dilute CH₂Cl₂/methanol/diethyl ether solution of **7** at 278 K to give a pale-yellow crystalline material (84 mg, 81%). ESI-MS (m/z): [M]⁺ 1635.20 (calcd 1635.19). ³¹P{¹H} NMR (CD₂Cl₂; 298 K; δ): AB₂ system 0.1 (br, 2P), -7.0 (br, 1P) [$^3J(P-P) = 141$ Hz]. ¹H NMR (CD₂Cl₂; 298 K; δ): PPh₂ groups 7.66 (m, 8H, $J(H-H) = 7.0$ Hz, $J(H-P) = 13.0$ Hz, *o*-H), 7.45 (m, 12H, *m*+*p*-H), 7.33 (t, 4H, $J(H-H) = 7.5$ Hz, *p*-H), 7.13 (dd, 8H, $J(H-H) = 6.7$

and 7.5 Hz, *m*-H), 6.70 (m, 8H, $J(\text{H-H}) = 6.7$ Hz, $J(\text{H-P}) = 12.0$ Hz, *o*-H); C_6H_4 7.76 (dm, 4H, $J(\text{H-H}) = 7.1$ Hz, *o*-H), 7.56 (dd, 4H, $J(\text{H-H}) = 7.5$ and 7.5 Hz, *m*-H), 7.47 (dm, 4H, $J(\text{H-H}) = 7.5$ Hz, *m*-H), 7.33 (m, 4H, *o*-H); PPh 7.40 (m, 2H, *p*-H), 7.34 (m, 4H, *m*-H), 7.20 (m, 4H, *o*-H). IR (KBr; $\nu(\text{CN})$; cm^{-1}): 2172. Anal. Calcd for $\text{C}_8\text{H}_{66}\text{Cu}_2\text{AuF}_3\text{N}_2\text{O}_3\text{P}_6\text{S}$: C, 58.49; H, 3.72; N, 1.56. Found: C, 58.20; H, 3.76; N, 1.85.

X-ray Structure Determinations. The crystals of 1–5 were immersed in cryo oil, mounted in a Nylon loop, and measured at a temperature of 120 K. The diffraction data were collected with Bruker SMART APEX II and Bruker Kappa Apex II Duo diffractometers using Mo $K\alpha$ radiation ($\lambda = 0.71073$ Å). The APEX2³⁰ program package was used for cell refinements and data reductions. The structures were solved by direct methods using the SHELXS-97 and SHELXS-2013³¹ programs with the WinGX³² graphical user interface. A semiempirical absorption correction (SADABS)³³ was applied to all data. Structural refinements were carried out using SHELXL-97 and SHELXL-2013.³¹

The structure of 4a was refined as an inversion twin. One of the CF_3SO_3^- counterions was disordered; however, no suitable disorder model was found. The displacement parameters of the F atoms of this moiety were constrained to be equal. The dichloromethane solvent molecule [C(175), Cl(5), and Cl(6)] in 4a was disordered between two sites and was refined with occupancies of 0.64/0.36. The displacement and geometric constraints and restraints were applied to both components.

The crystal of 5 was of low quality because of the presence of partially lost and heavily disordered crystallization solvent molecules as well as BF_4^- counterions. These reasons did not allow for high-quality refinement, and the structural data of 5 are presented in the Supporting Information only. Two of the BF_4^- anions were poorly defined and were refined with an occupancy of 0.5 at each site. A series of geometric and displacement restraints and constraints were applied to these moieties. The crystallization solvent was lost from the crystal and could not be resolved unambiguously. The contribution of the missing solvent to the calculated structure factors was taken into account by using a SQUEEZE routine of PLATON.³⁴ The missing solvent was not taken into account in the unit cell content.

All H atoms in 1–5 were positioned geometrically and constrained to ride on their parent atoms, with C–H = 0.95–0.99 Å, O–H = 0.84 Å, and $U_{\text{iso}} = 1.2U_{\text{eq}}$ (parent atom). The crystallographic details are summarized in Table S1.

Photophysical Measurements. Steady-state absorption and emission measurements were recorded on a Hitachi (U-3310) spectrophotometer and an Edinburgh (FS920) fluorimeter, respectively. Both the wavelength-dependent excitation and emission responses of the fluorimeter have been calibrated. To determine the photoluminescence quantum yield in solution, 4-(dicyanomethylene)-2-methyl-6- $[p$ -(dimethylamino)styryl]-4Hpyran (DCM; $\lambda_{\text{max}} = 615$ nm, exciton) in methanol with a quantum yield of 0.4 served as the standard for measuring the quantum yield. In the solid state, quantum yields were determined on a calibrated integrating sphere system (FLSP 920P; Edinburgh). The uncertainty of the quantum yield measurement was in the range of $\pm 5\%$ (an average of three replications, which correspond to different orientations of the sample). Lifetime studies were performed with an Edinburgh FL 900 photon-counting system using a hydrogen-filled lamp as the excitation source. The emission decays were fitted by the sum of the exponential functions with a temporal resolution of 300 ps by deconvolution of the instrument response function. The O_2 -sensing properties worked on the principle of luminescence intensity quenching. In this approach, a 405 nm laser line (diode laser, 405-50-COL-004, Oxiuss) was used as an excitation source throughout the measurement. A set of neutral density filters was then placed in the beam path to attenuate the laser power. N_2 (99.99%) and O_2 (99.99%) were mixed at different concentrations in mass-flow controllers and passed into a Linkam FTIR600 hot stage (Linkam Scientific Instruments). The microscope (Olympus BX51) had an upright-style frame in which all optics were modified to allow the passage of deep-UV to IR light. The output flow rate of the gas mixture was maintained at 500 mL/min. The O_2 concentrations were accurate to 0.1%. The luminescence was collected

by an optical assembly at the entrance slit of a polychromator (blazed at 500 nm) coupled with a sensitive charge-coupled detector (PI-MAX, Princeton Instruments).

Thermogravimetric analysis (TGA) of 4a and 4b was performed with a computer-controlled Dynamic Q500 (TA Instruments). Samples of 4a and 4b were loaded into platinum holders and heated with a ramp rate of 3 °C/min from room temperature to 800 °C in an airflow of 60 mL/min. Gas sorption isotherms were measured on a volumetric adsorption apparatus (Micromeritics ASAP 2020). The samples of 4a and 4b (weight about 250 mg) were in situ evacuated under a high vacuum at 373 K for 12 h prior to the sorption measurements.

Computational Details. The d^{10} complexes 1–7 were studied using DFT-PBE0.³⁵ All d^{10} metal atoms were described by a triple- ζ valence-quality basis set with polarization functions (def2-TZVP), while a split-valence basis set with polarization functions on non-H atoms was used for all other atoms [def2-SV(P)].³⁶ A multipole-accelerated resolution-of-the-identity technique was used to speed up the calculations.³⁷ To facilitate comparisons with the experiments, point-group symmetry was applied as follows: 1–6, C_1 ; 7, C_{2v} . The geometries of all complexes were fully optimized. The excited states were investigated with the TDDFT approach.³⁸ Singlet excitations were determined at the optimized ground-state S_0 geometries, while the lowest-energy triplet emissions were determined at the optimized T_1 geometry. The $T_1 \rightarrow S_0$ emission wavelengths predicted by TDDFT-PBE0 were grossly overestimated for complexes 1–6, and the data shown in Table 3 correspond to the HOMO–LUMO gaps at the optimized T_1 geometry. We tried to obtain the $T_1 \rightarrow S_0$ emission wavelengths also by using the high-level ab initio second-order approximate coupled-cluster method, which is an approximation of the coupled-cluster singles and doubles method.³⁹ However, the coupled-cluster equations showed a poor convergence behavior possibly because of large contributions from double excitations. Because of the relatively large size of the studied complexes, it is not currently feasible to apply even higher-level methods that would be required for a quantitative description of the T_1 state. All electronic structure calculations were carried out with the TURBOMOLE program package (version 6.5).⁴⁰

■ ASSOCIATED CONTENT

📄 Supporting Information

The Supporting Information is available free of charge on the ACS Publications website at DOI: 10.1021/acs.inorgchem.5b02581.

Additional NMR and ESI-MS data, crystal structures, bond lengths and angles, and TGA curves (PDF)

Optimized Cartesian coordinates of the studied systems in XYZ format (XYZ)

X-ray crystallographic data in CIF format for 1–5 (CIF)

■ AUTHOR INFORMATION

Corresponding Authors

*E-mail: chop@ntu.edu.tw (P.-T.C.).

*E-mail: meilin_ho@scu.edu.tw (M.-L.H.).

*E-mail: igor.koshevoy@uef.fi (I.O.K.).

Notes

The authors declare no competing financial interest.

■ ACKNOWLEDGMENTS

Financial support from the University of Eastern Finland (Russian–Finnish collaborative project), the Academy of Finland (Grant 268993 to I.O.K.), the Alfred Kordelin Foundation (to A.J.K.), and the Russian Foundation for Basic Research (Grants 13-04-40342 and 13-03-12411) is gratefully acknowledged. Computational resources were provided by CSC, the Finnish IT Center for Science (to A.J.K.).

REFERENCES

- (1) (a) Barbieri, A.; Accorsi, G.; Armaroli, N. *Chem. Commun.* **2008**, 2185–2193. (b) Yam, V. W.-W.; Wong, K. M.-C. *Chem. Commun.* **2011**, 47, 11579–11592. (c) He, X.; Yam, V. W.-W. *Coord. Chem. Rev.* **2011**, 255, 2111–2123. (d) Yersin, H.; Rausch, A. F.; Czerwieńiec, R.; Hofbeck, T.; Fischer, T. *Coord. Chem. Rev.* **2011**, 255, 2622–2652. (e) Lima, J. C.; Rodriguez, L. *Chem. Soc. Rev.* **2011**, 40, 5442–5456. (f) Wenger, O. S. *Chem. Rev.* **2013**, 113, 3686–3733. (g) Zink, D. M.; Volz, D.; Baumann, T.; Mydlak, M.; Flugge, H.; Friedrichs, J.; Nieger, M.; Bräse, S. *Chem. Mater.* **2013**, 25, 4471–4448. (h) Osawa, M.; Kawata, I.; Ishii, R.; Igawa, S.; Hashimoto, M.; Hoshino, M. *J. Mater. Chem. C* **2013**, 1, 4375–4383. (i) Jobbágy, C.; Deák, A. *Eur. J. Inorg. Chem.* **2014**, 2014, 4434–4449. (j) Langdon-Jones, E. E.; Pope, S. J. A. *Chem. Commun.* **2014**, 50, 10343–10354. (k) Wallesch, M.; Volz, D.; Zink, D. M.; Schepers, U.; Nieger, M.; Baumann, T.; Bräse, S. *Chem. - Eur. J.* **2014**, 20, 6578–6590. (l) Yam, V. W.-W.; Au, V. K.-M.; Leung, S. Y.-L. *Chem. Rev.* **2015**, 115, 7589–7728.
- (2) (a) Schmidbaur, H.; Schier, A. *Chem. Soc. Rev.* **2008**, 37, 1931–1951. (b) Tiekink, E. R. T.; Kang, J.-G. *Coord. Chem. Rev.* **2009**, 253, 1627–1648. (c) Schmidbaur, H.; Schier, A. *Chem. Soc. Rev.* **2012**, 41, 370–412.
- (3) (a) Henary, M.; Zink, J. I. *Inorg. Chem.* **1991**, 30, 3111–3112. (b) Brasse, C.; Raithby, P. R.; Rennie, M.-A.; Russell, C. A.; Steiner, A.; Wright, D. S. *Organometallics* **1996**, 15, 639–644. (c) Dyason, J. C.; Healy, P. C.; Engelhardt, L. M.; Pakawatchai, C.; Patrick, V. A.; Raston, C. L.; White, A. H. *J. Chem. Soc., Dalton Trans.* **1985**, 831–838. (d) Yam, V. W.-W.; Lee, W.-K.; Cheung, K.-K. *J. Chem. Soc., Dalton Trans.* **1996**, 2335–2339.
- (4) Maini, L.; Braga, D.; Mazzeo, P. P.; Ventura, B. *Dalton Trans.* **2012**, 41, 531–539.
- (5) (a) Ford, P. C.; Cariati, E.; Bourassa, J. *Chem. Rev.* **1999**, 99, 3625–3647. (b) Li, S.-L.; Zhang, X.-M. *Inorg. Chem.* **2014**, 53, 8376–8383. (c) Naik, S.; Mague, J. T.; Balakrishna, M. S. *Inorg. Chem.* **2014**, 53, 3864–3873. (d) Bai, S.-Q.; Jiang, L.; Young, D. J.; Hor, T. S. A. *Dalton Trans.* **2015**, 44, 6075–6081. (e) Knorr, M.; Bonnot, A.; Lapprand, A.; Khatyr, A.; Strohmman, C.; Kubicki, M. M.; Rousselin, Y.; Harvey, P. D. *Inorg. Chem.* **2015**, 54, 4076–4093. (f) Liu, W.; Fang, Y.; Wei, G. Z.; Teat, S. J.; Xiong, K.; Hu, Z.; Lustig, W. P.; Li, J. *J. Am. Chem. Soc.* **2015**, 137, 9400–9408.
- (6) (a) Tard, C.; Perruchas, S.; Maron, S.; Le Goff, X. F.; Guillen, F.; Garcia, A.; Vigneron, J.; Etcheberry, A.; Gacoin, T.; Boilot, J.-P. *Chem. Mater.* **2008**, 20, 7010–7016. (b) Kitagawa, H.; Ozawa, Y.; Toriumi, K. *Chem. Commun.* **2010**, 46, 6302–6304. (c) Perruchas, S.; Le Goff, X. F.; Maron, S.; Maurin, I.; Guillen, F.; Garcia, A.; Gacoin, T.; Boilot, J.-P. *J. Am. Chem. Soc.* **2010**, 132, 10967–10969. (d) Wang, J.-H.; Li, M.; Zheng, J.; Huang, X.-C.; Li, D. *Chem. Commun.* **2014**, 50, 9115–9118. (e) Benito, Q.; Le Goff, X. F.; Maron, S. b.; Fargues, A.; Garcia, A.; Martineau, C.; Taulelle, F.; Kahlal, S.; Gacoin, T.; Boilot, J.-P.; Perruchas, S. *J. Am. Chem. Soc.* **2014**, 136, 11311–11320. (f) Cho, S.; Jeon, Y.; Lee, S.; Kim, J.; Kim, T. H. *Chem. - Eur. J.* **2015**, 21, 1439–1443. (g) Hayashi, T.; Kobayashi, A.; Ohara, H.; Yoshida, M.; Matsumoto, T.; Chang, H.-C.; Kato, M. *Inorg. Chem.* **2015**, 54, 8905–8913. (h) Benito, Q.; Le Goff, X. F.; Nocton, G.; Fargues, A.; Garcia, A.; Berhault, A. I.; Kahlal, S.; Saillard, J.-Y.; Martineau, C.; Trébosc, J.; Gacoin, T.; Boilot, J.-P.; Perruchas, S. *Inorg. Chem.* **2015**, 54, 4483–4494. (i) Benito, Q.; Baptiste, B.; Polian, A.; Delbes, L.; Martinelli, L.; Gacoin, T.; Boilot, J.-P.; Perruchas, S. *Inorg. Chem.* **2015**, 54, 9821–9825.
- (7) (a) Hashimoto, M.; Igawa, S.; Yashima, M.; Kawata, I.; Hoshino, M.; Osawa, M. *J. Am. Chem. Soc.* **2011**, 133, 10348–10351. (b) Zhang, Q.; Komino, T.; Huang, S.; Matsunami, S.; Goushi, K.; Adachi, C. *Adv. Funct. Mater.* **2012**, 22, 2327–2336. (c) Igawa, S.; Hashimoto, M.; Kawata, I.; Yashima, M.; Hoshino, M.; Osawa, M. *J. Mater. Chem. C* **2013**, 1, 542–551. (d) Chen, X.-L.; Yu, R.; Zhang, Q.-K.; Zhou, L.-J.; Wu, X.-Y.; Zhang, Q.; Lu, C.-Z. *Chem. Mater.* **2013**, 25, 3910–3920. (e) Osawa, M.; Hoshino, M.; Hashimoto, M.; Kawata, I.; Igawa, S.; Yashima, M. *Dalton Trans.* **2015**, 44, 8369–8378.
- (8) (a) Zhao, Q.; Li, F.; Huang, C. *Chem. Soc. Rev.* **2010**, 39, 3007–3030. (b) Smith, C. S.; Mann, K. R. *J. Am. Chem. Soc.* **2012**, 134, 8786–8789. (c) Zhou, Y.-P.; Liu, E.-B.; Wang, J.; Chao, H.-Y. *Inorg. Chem.* **2013**, 52, 8629–8637.
- (9) (a) Lotito, K. J.; Peters, J. C. *Chem. Commun.* **2010**, 46, 3690–3692. (b) Czerwieńiec, R.; Yu, J.; Yersin, H. *Inorg. Chem.* **2011**, 50, 8293–8301. (c) Wada, A.; Zhang, Q.; Yasuda, T.; Takasu, I.; Enomoto, S.; Adachi, C. *Chem. Commun.* **2012**, 48, 5340–5342. (d) Zink, D. M.; Bächle, M.; Baumann, T.; Nieger, M.; Kühn, M.; Wang, C.; Klopfer, W.; Monkowius, U.; Hofbeck, T.; Yersin, H.; Bräse, S. *Inorg. Chem.* **2013**, 52, 2292–2305. (e) Krylova, V. A.; Djurovich, P. L.; Conley, B. L.; Haiges, R.; Whited, M. T.; Williams, T. J.; Thompson, M. E. *Chem. Commun.* **2014**, 50, 7176–7179.
- (10) Lavie-Cambot, A.; Cantuel, M.; Leydet, Y.; Jonusauskas, G.; Bassani, D. M.; McClenaghan, N. D. *Coord. Chem. Rev.* **2008**, 252, 2572–2584.
- (11) (a) Cuttall, D. G.; Kuang, S.-M.; Fanwick, P. E.; McMillin, D. R.; Walton, R. A. *J. Am. Chem. Soc.* **2002**, 124, 6–7. (b) McCormick, T.; Jia, W.-L.; Wang, S. *Inorg. Chem.* **2006**, 45, 147–155. (c) Crestani, M. G.; Manbeck, G. F.; Brennessel, W. W.; McCormick, T. M.; Eisenberg, R. *Inorg. Chem.* **2011**, 50, 7172–7188. (d) Czerwieńiec, R.; Kowalski, K.; Yersin, H. *Dalton Trans.* **2013**, 42, 9826–9830. (e) Bergmann, L.; Friedrichs, J.; Mydlak, M.; Baumann, T.; Nieger, M.; Bräse, S. *Chem. Commun.* **2013**, 49, 6501–6503.
- (12) (a) Miller, A. J. M.; Dempsey, J. L.; Peters, J. C. *Inorg. Chem.* **2007**, 46, 7244–7246. (b) Hsu, C.-W.; Lin, C.-C.; Chung, M.-W.; Chi, Y.; Lee, G.-H.; Chou, P.-T.; Chang, C.-H.; Chen, P.-Y. *J. Am. Chem. Soc.* **2011**, 133, 12085–12099.
- (13) (a) Osawa, M.; Hoshino, M. *Chem. Commun.* **2008**, 6384–6386. (b) Igawa, S.; Hashimoto, M.; Kawata, I.; Hoshino, M.; Osawa, M. *Inorg. Chem.* **2012**, 51, 5805–5813. (c) Kaeser, A.; Moudam, O.; Accorsi, G.; Séguy, I.; Navarro, J.; Belbakra, A.; Duhayon, C.; Armaroli, N.; Delavaux-Nicot, B.; Nierengarten, J.-F. *Eur. J. Inorg. Chem.* **2014**, 2014, 1345–1355.
- (14) (a) Hu, J.; Nguyen, M.-H.; Yip, J. H. K. *Inorg. Chem.* **2011**, 50, 7429–7439. (b) Zhang, J.; Yang, Q.; Zhu, Y.; Liu, H.; Chi, Z.; Su, C.-Y. *Dalton Trans.* **2014**, 43, 15785–15790.
- (15) Crespo, O.; Gimeno, M. C.; Laguna, A.; Marriott, R.; Sáez-Rocher, J. M.; Villacampa, M. D. *Dalton Trans.* **2014**, 43, 12214–12220.
- (16) Chakkaradhari, G.; Belyaev, A. A.; Karttunen, A. J.; Sivchik, V.; Tunik, S. P.; Koshevoy, I. O. *Dalton Trans.* **2015**, 44, 13294–13300.
- (17) (a) Lin, Y.-Y.; Lai, S.-W.; Che, C.-M.; Fu, W.-F.; Zhou, Z.-Y.; Zhu, N. *Inorg. Chem.* **2005**, 44, 1511–1524. (b) Tsuboyama, A.; Kuge, K.; Furugori, M.; Okada, S.; Hoshino, M.; Ueno, K. *Inorg. Chem.* **2007**, 46, 1992–2001. (c) Ray, M. J.; Randall, R. A. M.; Arachchige, K. S. A.; Slawin, A. M. Z.; Bühl, M.; Lebl, T.; Kilian, P. *Inorg. Chem.* **2013**, 52, 4346–4359.
- (18) Zank, J.; Schier, A.; Schmidbaur, H. *J. Chem. Soc., Dalton Trans.* **1999**, 415–420.
- (19) Celik, M. A.; Dash, C.; Adiraju, V. A. K.; Das, A.; Yousufuddin, M.; Frenking, G.; Dias, H. V. R. *Inorg. Chem.* **2013**, 52, 729–742.
- (20) (a) Zhao, Y.; Hong, M.; Su, W.; Cao, R.; Zhou, Z.; Chan, A. S. C. *J. Chem. Soc., Dalton Trans.* **2000**, 1685–1686. (b) Katz, M. J.; Rammial, T.; Yu, H.-Z.; Leznoff, D. B. *J. Am. Chem. Soc.* **2008**, 130, 10662–10673. (c) Jobbágy, C.; Tunyogi, T.; Palinkas, G.; Deak, A. *Inorg. Chem.* **2011**, 50, 7301–7308. (d) Liu, Y.-l.; Han, L.-j.; Qiao, G.-R.; Yang, M.; Zhang, Q.; Wang, J.-g.; Zhan, S.-z. *Synth. React. Inorg. Met.-Org., Nano-Met. Chem.* **2012**, 42, 183–189. (e) Kitazawa, T.; Hiruma, K.; Sato, H.; Tamura, K.; Yamagishi, A. *Dalton Trans.* **2013**, 42, 16680–16682. (f) Ahern, J. C.; Roberts, R. J.; Follansbee, P.; McLaughlin, J.; Leznoff, D. B.; Patterson, H. H. *Inorg. Chem.* **2014**, 53, 7571–7579. (g) Vreshch, V.; Shen, W.; Nohra, B.; Yip, S.-K.; Yam, V. W.-W.; Lescop, C.; Reau, R. *Chem. - Eur. J.* **2012**, 18, 466–477. (h) Vreshch, V.; Nohra, B.; Lescop, C.; Reau, R. *Inorg. Chem.* **2013**, 52, 1496–1503.
- (21) Ho, M.-L.; Shih, C.-H.; Lee, C.-H.; Lee, G.-H. *CrystEngComm* **2011**, 13, 992–1002.
- (22) Cunningham, C. T.; Moore, J. J.; Cunningham, K. L. H.; Fanwick, P. E.; McMillin, D. R. *Inorg. Chem.* **2000**, 39, 3638–3644.

(23) (a) Hofbeck, T.; Monkowius, U.; Yersin, H. *J. Am. Chem. Soc.* **2015**, *137*, 399–404. (b) Linfoot, C. L.; Leitel, M. J.; Richardson, P.; Rausch, A. F.; Chepelin, O.; White, F. J.; Yersin, H.; Robertson, N. *Inorg. Chem.* **2014**, *53*, 10854–10861.

(24) Englman, R.; Jortner, J. *Mol. Phys.* **1970**, *18*, 145–164.

(25) (a) Wang, Y.; Li, B.; Liu, Y.; Zhang, L.; Zuo, Q.; Shi, L.; Su, Z. *Chem. Commun.* **2009**, 5868–5870. (b) Wang, X.-d.; Wolfbeis, O. S. *Chem. Soc. Rev.* **2014**, *43*, 3666–3761. (c) Medina-Rodriguez, S.; Orriach-Fernandez, F. J.; Poole, C.; Kumar, P.; de la Torre-Vega, A.; Fernandez-Sanchez, J. F.; Baranoff, E.; Fernandez-Gutierrez, A. *Chem. Commun.* **2015**, *51*, 11401–11404.

(26) (a) Smith, C. S.; Branham, C. W.; Marquardt, B. J.; Mann, K. R. *J. Am. Chem. Soc.* **2010**, *132*, 14079–14085. (b) Liu, S.-Y.; Qi, X.-L.; Lin, R.-B.; Cheng, X.-N.; Liao, P.-Q.; Zhang, J.-P.; Chen, X.-M. *Adv. Funct. Mater.* **2014**, *24*, 5866–5872.

(27) (a) McGee, K. A.; Mann, K. R. *J. Am. Chem. Soc.* **2009**, *131*, 1896–1902. (b) Medina-Rodriguez, S.; Marin-Suarez, M.; Fernandez-Sanchez, J. F.; de la Torre-Vega, A.; Baranoff, E.; Fernandez-Gutierrez, A. *Analyst* **2013**, *138*, 4607–4617. (c) Li, M.; Zheng, B.; Luo, D.; Sun, H.; Wang, N.; Huang, Y.; Dai, J.; Xiao, D.; Su, S.-J.; Lu, Z. *Chem. Commun.* **2015**, *51*, 1926–1929.

(28) Luo, X.; Zhang, H.; Duan, H.; Liu, Q.; Zhu, L.; Zhang, T.; Lei, A. *Org. Lett.* **2007**, *9*, 4571–4574.

(29) Hartley, J. G.; Venanzi, L. M.; Goodall, D. C. *J. Chem. Soc.* **1963**, 3930–3936.

(30) APEX2: *Software Suite for Crystallographic Programs*; Bruker AXS, Inc.: Madison, WI, 2009.

(31) Sheldrick, G. M. *Acta Crystallogr., Sect. C: Struct. Chem.* **2015**, *71*, 3–8.

(32) Farrugia, L. J. *J. Appl. Crystallogr.* **1999**, *32*, 837–838.

(33) Sheldrick, G. M. *SADABS-2008/1: Bruker AXS area detector scaling and absorption correction*; Bruker AXS: Madison, WI, 2008.

(34) Spek, A. L. *PLATON, A Multipurpose Crystallographic Tool*, version 1.17; Utrecht University: Utrecht, The Netherlands, 2011.

(35) Perdew, J. P.; Burke, K.; Ernzerhof, M. *Phys. Rev. Lett.* **1996**, *77*, 3865–3868.

(36) Weigend, F.; Ahlrichs, R. *Phys. Chem. Chem. Phys.* **2005**, *7*, 3297–3305.

(37) Eichkorn, K.; Treutler, O.; Öhm, H.; Häser, M.; Ahlrichs, R. *Chem. Phys. Lett.* **1995**, *240*, 283–290.

(38) Furche, F.; Rappoport, D. *Density Functional Methods for Excited States: Equilibrium Structure and Electronic Spectra*. In *Computational Photochemistry*; Olivucci, M., Ed.; Elsevier: Amsterdam, The Netherlands, 2005; pp 93–128.

(39) Christiansen, O.; Koch, H.; Jørgensen, P. *Chem. Phys. Lett.* **1995**, *243*, 409–418.

(40) Ahlrichs, R.; Bär, M.; Häser, M.; Horn, H.; Kölmel, C. *Chem. Phys. Lett.* **1989**, *162*, 165–169.